2007 IEEE International Conference on
Robotics and Automation
Roma, Italy, 10-14 April 2007

ZMP-based Biped Running Enhanced by Toe Springs

Shuuji KAJITA, Kenji KANEKO, Mitsuharu MORISAWA,
Shinichiro NAKAOKA and Hirohisa HIRUKAWA
Intelligent Systems Research Institute, AIST
1-1-1 Umezono, Tsukuba, Ibaraki, 305-8568 Japan
{s.kajita,k.kaneko,m.morisawa,s.nakaoka,hiro.hirukawa}@aist.go.jp

***Abstract*— We discuss a ZMP-based running pattern generation for a biped robot equipped with toe springs. Our biped robot HRP-2LT has twelve active DoFs for its legs and two passive DoFs for its toes. The trajectory of the center of mass is designed to realize the specified running motion and the foot trajectories are determined to get proper spring action at lift off phases. They are interpreted into joint angles by using the resolved momentum control. By the simulation and the preliminary experiment, it is shown that the toe springs are effectively used for running and hopping.**

I. INTRODUCTION

Recently, many humanoid projects focus on biped walking as an important subject and have already demonstrated reliable dynamic biped walking [1]–[6]. As the next step of development, it might be natural to consider the realization of biped running. We believe it is a worthwhile technical challenge for the following reasons. First, studying robot running will add new functions of mobility to humanoid robots. For example, jumping over large obstacles or a crevasse in the ground might be realized by a derivative of running control. Second, studying extreme situations will give us insights to improve the hardware itself. Current robots are too fragile to operate in any environment. Even when the robot operates at low speed, we must treat them carefully. We hope to overcome this fragility in the process of developing a running humanoid.

Running robots have been intensively studied by Raibert and his colleagues [7]. Their famous hopping robots driven by pneumatic and hydraulic actuators performed various actions including somersaults [8]. Using a similar control strategy, Hodgins simulated a running human in the computer graphics [9]. Ahmadi and Buehler studied running monopods from a standpoint of energy efficiency [10]. Their ARL Monopod II is an electrically powered running robot of 18 [kg] weight and could run at 4.5 [km/h] with a power expenditure of only 48 [W].

All of those robots have a spring mechanism to retrieve kinetic energy during running cycles. It is obvious that these springs help running but they might prevent ordinary humanoid activities such as walking, carrying objects and so on. From this reason, some researchers have considered to realize running by using bipeds/humanoids without springs. The first humanoid robot running was realized by Nagasaka et al. [11] in 2003. His robot QRIO was a self-contained 38 DoF humanoid, 580 [mm] height, 7 [kg] weight, and demonstrated running at 0.83 [km/h]. Following Nagasaka, the authors have also realized running of 0.58 [km/h] using 12 DoF, 1.27[m], 31.0 [kg] humanoid biped HRP-2LR [12]. Chevallereau, Westerbelt and Grizzle reported the biped running of RABBIT robot which has point feet [13]. Currently, the fastest biped humanoid robot is Honda's ASIMO which can run at 6[km/h] announced on December 13, 2005[1].

To improve the running speed of HRP-2LR we add springy toe joints and call it HRP-2LT (Fig. 1). In this paper, its running pattern generation is mainly discussed. We introduce a method to generate the joint trajectories including passive spring joint based on the reference Zero-Moment Point(ZMP), although the conventional ZMP scheme requires all joints to be position controlled [14].

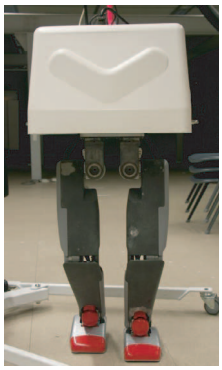

(a) HRP-2LT

(b) Feet equipped with toe springs

Fig. 1. HRP-2LT: 12 DoF biped robot with toe springs

The rest part of this paper is organized as following. In Section II, our biped robot HRP-2LT and its feet with toe springs are explained. Section III discusses the planning of the center of mass and the ZMP, then in Section IV, the feet trajectories to utilize the toe springs is described in detail. In Section V, we explain the method to transform the trajectories obtained in the preceding section into joint angles. Then in Section VI, we show the effectiveness of toe springs in terms of the joint speed limitations. The early stage of simulations and the experiment is shown in Section VII. We conclude this paper and address our future plans in Section VIII.

[1]The technical details of the running ASIMO are not yet disclosed, however, it is most likely that ZMP is used for it. On the other hand, we cannot tell whether ASIMO is equipped with spring mechanisms or not. (http://world.honda.com/ASIMO)

1-4244-0602-1/07/$20.00 ©2007 IEEE.

II. Running robot hardware

A. HRP-2LT

We replaced the feet of HRP-2LR, the biped robot which realized running in 2004, with the new feet with toe springs. The robot and its feet are shown in Fig. 1, and we call this robot HRP-2LT. Adding a new mechanism to the feet, the total mass of the robot became 32.3[kg], a little bit heavier than the original.

B. Foot with toe spring

The expected role of the toe springs are to accumulate and release energy during running. To estimate an appropriate parameter, we simulated a robot fall down from a few centimeters high as shown in Fig. 2.

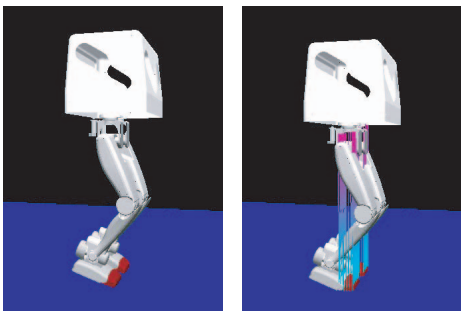

(a) Initial state of falling (b) Touchdown with toe bending

Fig. 2. Simulation to determine the foot spring constant

Figure 3 shows the simulated toe bend with different spring constants [2]. With 50 [Nm/rad], the robot just settled on the ground (thin line). With spring constant of 100 [Nm/rad], the robot bounced several times (bold line). With 300 [Nm/rad] the robot sharply bounced and left ground again (dashed line). We assumed that the second setting will be suitable for our purpose.

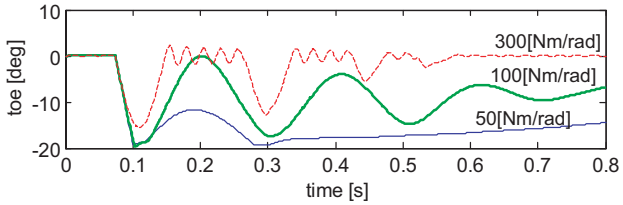

Fig. 3. Simulated behavior of springy toe

Torsion springs were designed to realize the specified spring constant. Their final specifications are shown in Table I. The foot mechanism with the springy toe joint is shown in Fig.4(a). We assigned two torsion springs in parallel for one foot and the bending angle of the passive joint is measured by a small rotary encoder. The maximum bending angle of the toe joint is 42 [deg] which is shown in Fig.4(b).

[2]We gave a half of the spring constant for each toe spring, since the robot hops with both of toes while we want to specify the single leg behavior.

TABLE I
TOE SPRING SPECIFICATION

Material	Piano wire type B (SWPB)
Turns	4
Coil diam. average	30 [mm]
Wire diam.	6 [mm]
Spring const. (by two)	64.6 [Nm/rad]

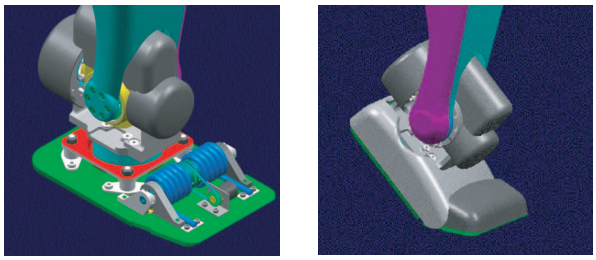

(a) Toe spring mechanism (b) Maximum toe bending

Fig. 4. Foot mechanism with spring

III. Planning of center of mass trajectory

A. Vertical CoM motion

To specify the vertical hopping motion, we first determined the support period and the flight period to be $T_s = 0.3$[s] and $T_f = 0.06$[s] respectively. Next we designed the corresponding profiles of the floor reaction force and the trajectory of the center of mass (CoM). Figure 5 shows the vertical floor reaction force (upper graph) and the CoM (lower graph) for a motion of three times hopping. The vertical floor force is designed to decrease by quadratic curve before the lift-off, since we could get a reliable hopping motion by this way in our previous experiments [15]. The starting and the finishing CoM motion is interpolated by using the fifth order polynomial to obtain trajectories which have continuous position, velocity and acceleration.

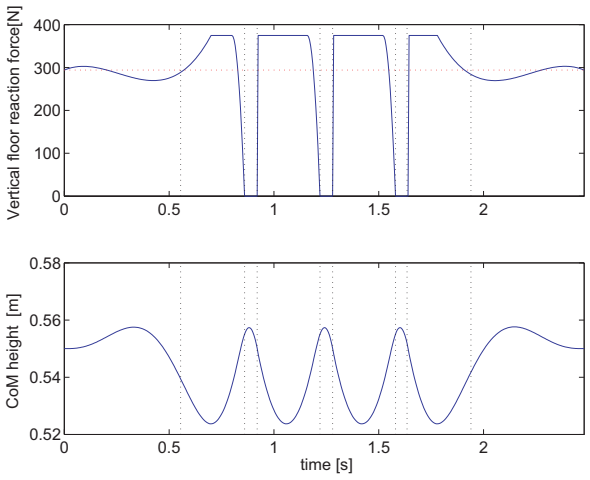

Fig. 5. Vertical reaction force and CoM motion

B. ZMP and horizontal CoM motion

Figure 6 illustrates the relationship between the ZMP and the toe bending in a single support. In the graph of ZMP,

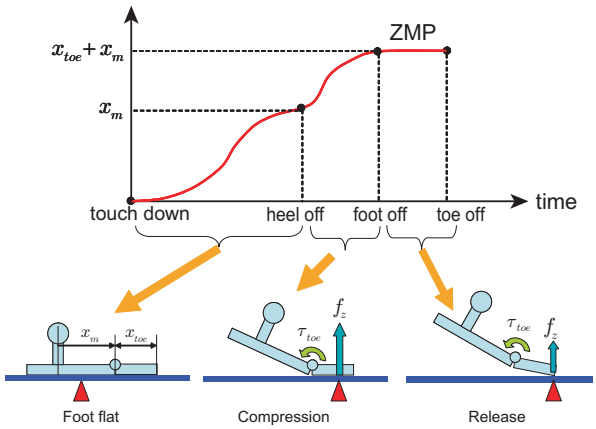

Fig. 6. ZMP and toe bending

x_m is the position of the toe joint with respect to the ankle and x_{toe} is the length of the toe link.

A single support can be separated into three phases.

1) **Foot flat phase:** ZMP moves from the foot center (below of the ankle joint) to the toe joint. Whole foot is on the floor during this period (touch down - heel off).
2) **Compression phase:** ZMP moves from the toe joint to the tiptoe. The torsion spring is compressed by The torque τ_{toe} around the toe joint, which results the heel rise (heel off - foot off).
3) **Release phase:** ZMP remains on the tiptoe. The toe link starts to rotate around the tiptoe, and the spring is released. At the moment of full toe extension, the robot gets lift off (foot off - toe off).

Assuming the robot phase changes in this order, we designed the ZMP trajectory and calculated the corresponding center of mass (CoM) trajectory by using Nishiwaki and Kagami's method [16]. Figure 7 shows the ZMP and the CoM trajectories for a running of three steps. In this graph, we indicate the ZMP in flight phase to be the projection of the CoM, while the ZMP of flying robot is not determined.

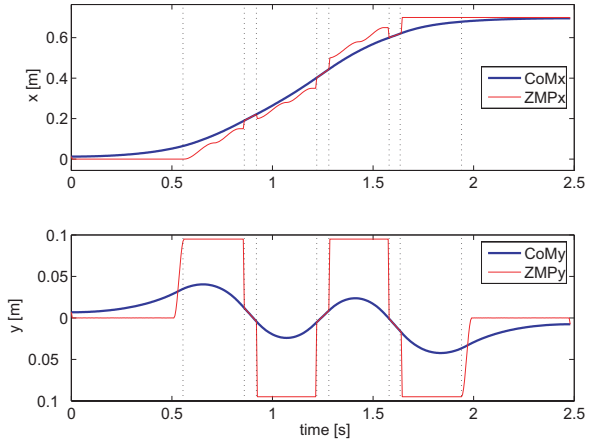

Fig. 7. Planned ZMP and CoM

IV. Planning Foot Trajectory

To calculate the toe bending of support phase, we assume a robot model of Fig.8 which consists of the CoM and the massless foot with a toe spring. For the simplicity, we discuss a 2D model which is a projection of the 3D model onto the sagittal plane.

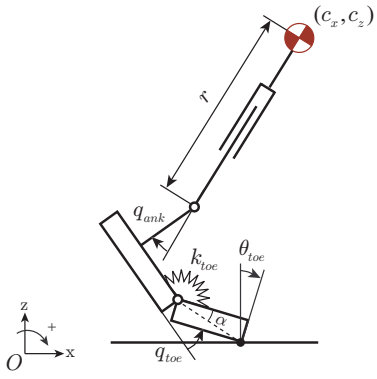

Fig. 8. CoM and support foot state

We assume the tiptoe is on the ground and represent the state vector as

$$\boldsymbol{\theta} := \begin{bmatrix} \theta_{toe} \\ q_{toe} \\ q_{ank} \\ r \end{bmatrix}, \tag{1}$$

where θ_{toe} is the rotation of the toe link and q_{toe} is the bending angle of the toe joint. During foot flat phase, we have $\theta_{toe} = q_{toe} = 0$. q_{ank} and r are the virtual ankle joint and the virtual leg length to simply represent the relationship between the foot and the CoM. The state vector and the CoM are connected by

$$\begin{bmatrix} \dot{c}_x \\ \dot{c}_z \end{bmatrix} = \boldsymbol{J}_c \dot{\boldsymbol{\theta}}. \tag{2}$$

where $\boldsymbol{J}_c$ is the CoM Jacobian.

The toe spring generates the torque τ_{toe} determined by

$$\tau_{toe} = k_{toe} q_{toe} \tag{3}$$

where k_{toe} is the toe spring constant.

A. Compression phase

In compression phase, the toe link is in full contact with the ground, thus $\theta_{toe} = 0$. Let us represent the ZMP location as (α_p, r_p) with respect to the toe joint as shown in Fig.9(a). The torque generated by the floor reaction force f is given by

$$\tau_{toe} = -r_p f \cos(\alpha_p - \theta_f), \tag{4}$$

where θ_f is the angle of reaction force from the vertical axis. From eqs.(3) and (4), we can calculate the toe bending as the following equation [17].

$$q_{toe} = -(r_p / k_{toe}) f \cos(\alpha_p - \theta_f) \tag{5}$$

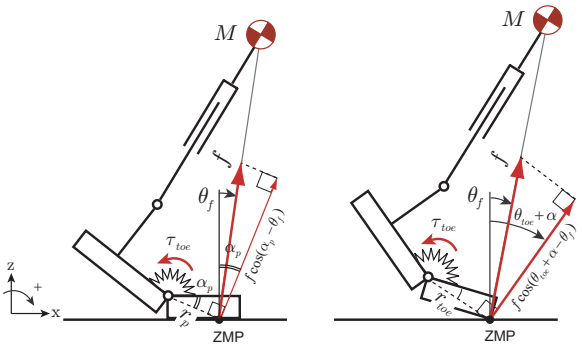

(a) Compression phase ($\theta_{toe}=0$) (b) Release phase

Fig. 9. Floor reaction force

B. Release phase

When the ZMP reaches the tiptoe, the toe link starts rotation as shown in Fig.9(b). In this phase, we must determine the angle of toe link θ_{toe} as well as the toe bending angle q_{toe}. Since we have four state variables as determined in eq. (1) against three constraints about c_x, c_z and f, we must handle the redundancy.

With given floor reaction force f, the toe joint torque is calculated as

$$\tau_{toe} = -r_{toe} f \cos(\theta_{toe} + \alpha - \theta_f), \tag{6}$$

where r_{toe} is the distance between the toe joint and the tiptoe and α is the angle of the toe tip with respect to the toe joint. The angle θ_f indicates the direction of the floor reaction force which points the CoM $[c_x\ c_z]^T$ since we are assuming a point mass model.

$$\theta_f = \tan^{-1}(c_x/c_z) \tag{7}$$

By substituting eq.(3) into above equation, we obtain

$$q_{toe} = -(r_{toe}/k_{toe}) f \cos(\theta_{toe} + \alpha - \theta_f) \tag{8}$$

Unlike in compression phase, we cannot get the solution since we still have θ_{toe} unknown.

Let us solve eq.(8) for the magnitude of the force f.

$$f = \left(\frac{k_{toe}}{r_{toe}}\right) \frac{-q_{toe}}{\cos(\theta_{toe} + \alpha - \theta_f)}, \tag{9}$$

By differentiating this, we obtain

$$\begin{aligned} \dot{f} &= \left[\frac{\partial f}{\partial \theta_{toe}} \ \frac{\partial f}{\partial q_{toe}} \ \frac{\partial f}{\partial \theta_f}\right] \begin{bmatrix} \dot{\theta}_{toe} \\ \dot{q}_{toe} \\ \dot{\theta}_f \end{bmatrix} \\ &=: [J_{f1}\ J_{f2}\ J_{f3}] \begin{bmatrix} \dot{\theta}_{toe} \\ \dot{q}_{toe} \\ \dot{\theta}_f \end{bmatrix}. \end{aligned} \tag{10}$$

Also, we obtain $\dot{\theta}_f$ by differentiating eq.(7).

$$\begin{aligned} \dot{\theta}_f &= \left[\frac{c_z}{c_x^2 + c_z^2} \ \frac{-c_x}{c_x^2 + c_z^2}\right] \begin{bmatrix} \dot{c}_x \\ \dot{c}_z \end{bmatrix} \\ &=: \boldsymbol{J}_{\theta f} \begin{bmatrix} \dot{c}_x \\ \dot{c}_z \end{bmatrix}. \end{aligned} \tag{11}$$

By substituting this into eq. (10), we get

$$\dot{f} = [J_{f1}\ J_{f2}] \begin{bmatrix} \dot{\theta}_{toe} \\ \dot{q}_{toe} \end{bmatrix} + J_{f3} \boldsymbol{J}_{\theta f} \begin{bmatrix} \dot{c}_x \\ \dot{c}_z \end{bmatrix}. \tag{12}$$

Finally, by using the CoM Jacobian (2) we get the relationship between the floor reaction force and the state vector.

$$\begin{aligned} \dot{f} &= [[J_{f1}, J_{f2}, 0, 0] + J_{f3} \boldsymbol{J}_{\theta f} \boldsymbol{J}_c] \dot{\boldsymbol{\theta}} \\ &=: \boldsymbol{J}_f \dot{\boldsymbol{\theta}}, \end{aligned} \tag{13}$$

where $\boldsymbol{J}_f$ represents the relationship between the robot state and the floor force. Let us call it the *Reaction Force Jacobian*.

By combining the CoM Jacobian (2) and the Reaction Force Jacobian (13), we get

$$\begin{bmatrix} \dot{c}_x \\ \dot{c}_z \\ \dot{f} \end{bmatrix} = \begin{bmatrix} \boldsymbol{J}_c \\ \boldsymbol{J}_f \end{bmatrix} \dot{\boldsymbol{\theta}} \tag{14}$$

From this equation, we can calculate the joint velocities for the given CoM speed and the rate of floor reaction force.

$$\dot{\boldsymbol{\theta}} = \begin{bmatrix} \boldsymbol{J}_c \\ \boldsymbol{J}_f \end{bmatrix}^{\dagger} \begin{bmatrix} \dot{c}_x \\ \dot{c}_z \\ \dot{f} \end{bmatrix} \tag{15}$$

where $\dagger$ means the pseudo-inverse operator.

By integrating $\dot{\boldsymbol{\theta}}$ obtained from above equation, we can calculate the support foot motion which satisfies the given profiles of the CoM and the floor reaction force.

C. Example toe bending motion

Figure 10 shows the calculated foot motion based on the ZMP-CoM pattern of Fig. 7 and our algorithm. The upper graph shows the toe rotation θ_{toe} (thin line for the right, bold line for the left) and the toe bending q_{toe} (thin broken line for the right, bold broken line for the left). In this pattern, the robot takes the first jump with its left leg. The toe joint starts bending at the heel off (a). Approximately at the full bending, the toe link starts rotating about the tiptoe (b). Then, the toe joint quickly extends until fully stretched at the lift off (c). During swing phase, the toe and the foot moves as one link and their posture is returned to the level before the next touch down (d).

The lower graph shows the total floor reaction force by dotted line and the contribution of the toe springs (thin line for the right, bold line for the left). From this graph we can observe that the toe springs accumulate the power in the middle of the support phase and release their power before the lift off.

D. Ankle trajectory

The final process is to determine the foot trajectories for the running sequence. Let us denote instantaneous configuration of the foot link as $\boldsymbol{p}_i, \boldsymbol{R}_i$ where $\boldsymbol{p}_i$ is the ankle joint position and $\boldsymbol{R}_i$ is the 3×3 rotation matrix for the foot link. We represent both parameters in the world frame and use $i = 1$ for the right foot and $i = 2$ for the left foot. For support phase, we can determine $\boldsymbol{p}_i, \boldsymbol{R}_i$ from the state vector

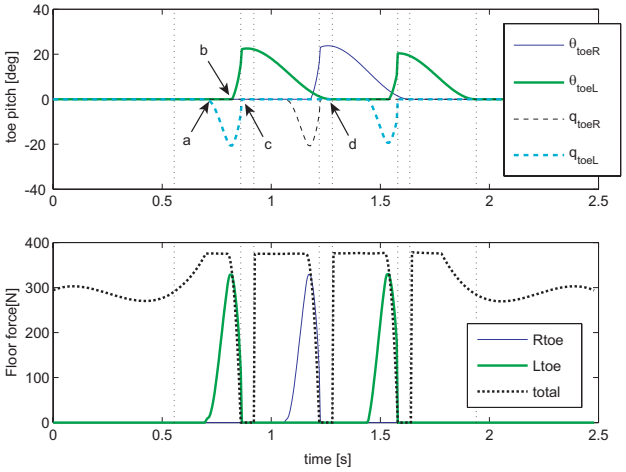

Fig. 10. Planned motion for toe springs

$\boldsymbol{\theta}$ (see Fig. 8). Swing phase trajectories are generated by interpolation of successive support phases. Figure 11 shows the left foot trajectory and the CoM of one complete running cycle calculated by this way.

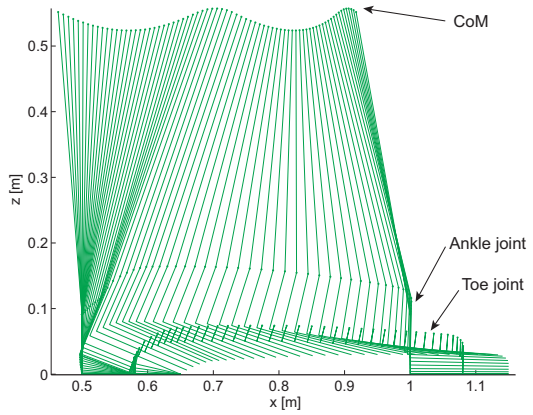

Fig. 11. Left foot and CoM for one complete running cycle

We also need the velocity of each foot in the next section. It is formally calculated as

$$\begin{aligned} \boldsymbol{v}_i &= \dot{\boldsymbol{p}}_i \\ \boldsymbol{\omega}_i &= (\dot{\boldsymbol{R}}_i \boldsymbol{R}_i^T)^\vee \end{aligned}$$

where the operator $\vee$ translates a skew symmetric matrix into a 3D vector.

V. Running Pattern Generation by Resolved Momentum Control

In this section, we calculate the trajectories of all joint angles which realizes the trajectories of the CoM and the foot determined in the last section. Let us determine the reference frames as Fig.12. With given velocity of the pelvis link frame $\boldsymbol{v}_B, \boldsymbol{\omega}_B$ and the frames of both ankles $\boldsymbol{v}_i, \boldsymbol{\omega}_i$ $(i = 1, 2)$, we can calculate the whole linear momentum $\mathcal{P}$ and the whole angular momentum around CoM $\mathcal{L}$ as following.

$$\begin{bmatrix} \mathcal{P} \\ \mathcal{L} \end{bmatrix} = \begin{bmatrix} \boldsymbol{M}_B \\ \boldsymbol{H}_B \end{bmatrix} \begin{bmatrix} \boldsymbol{v}_B \\ \boldsymbol{\omega}_B \end{bmatrix} + \begin{bmatrix} \mathcal{P}_{feet} \\ \mathcal{L}_{feet} \end{bmatrix} \tag{16}$$

$$\begin{bmatrix} \mathcal{P}_{feet} \\ \mathcal{L}_{feet} \end{bmatrix} := \sum_{i=1}^{2} \begin{bmatrix} \boldsymbol{M}_i \\ \boldsymbol{H}_i \end{bmatrix} \begin{bmatrix} \boldsymbol{v}_i \\ \boldsymbol{\omega}_i \end{bmatrix}$$

where $\boldsymbol{M}_*, \boldsymbol{H}_*$ are the inertia matrices which concern the constraint effects between the links.

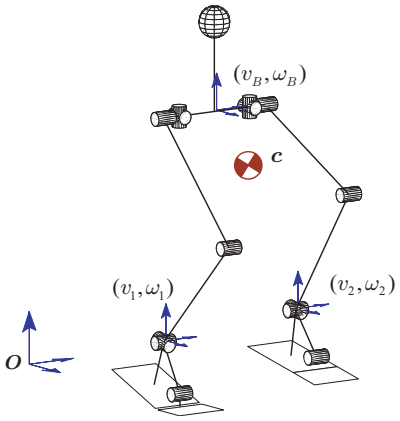

Fig. 12. Structure of HRP-2LT

We can determine the desired linear and angular momentum from the given CoM trajectory $\boldsymbol{c}(t)$ as

$$\mathcal{P}^d = M\dot{\boldsymbol{c}}, \ \mathcal{L}^d = 0. \tag{17}$$

By substituting them into eq.(16), we can obtain the desired pelvis velocity [18].

$$\begin{bmatrix} \boldsymbol{v}_B \\ \boldsymbol{\omega}_B \end{bmatrix} = \begin{bmatrix} \boldsymbol{M}_B \\ \boldsymbol{H}_B \end{bmatrix}^{-1} \begin{bmatrix} \mathcal{P}^d - \mathcal{P}_{feet} \\ \mathcal{L}^d - \mathcal{L}_{feet} \end{bmatrix} \tag{18}$$

However, this method tends to create unnatural rotation of the body since we forced the total angular momentum around CoM to be zero in eq.(17).

To avoid the deliberate assignment of the zero angular momentum and unnatural body motion, let us take notice of the angular momentum around projected CoM $\mathcal{L}_{x0}, \mathcal{L}_{y0}$ and the vertical linear momentum $\mathcal{P}_z$.

$$\begin{aligned} \begin{bmatrix} \mathcal{L}_{x0} \\ \mathcal{L}_{y0} \\ \mathcal{P}_z \end{bmatrix} &= \begin{bmatrix} 0 & -c_z & 0 \\ c_z & 0 & 0 \\ 0 & 0 & 1 \end{bmatrix} \mathcal{P} + \begin{bmatrix} 1 & 0 & 0 \\ 0 & 1 & 0 \\ 0 & 0 & 0 \end{bmatrix} \mathcal{L} \\ &=: \boldsymbol{S}_P \mathcal{P} + \boldsymbol{S}_L \mathcal{L} \end{aligned} \tag{19}$$

By multiplying the matrix $[\boldsymbol{S}_P \ \boldsymbol{S}_L]$ from the left of eq. (16),

$$\begin{aligned} \begin{bmatrix} \mathcal{L}_{x0} \\ \mathcal{L}_{y0} \\ \mathcal{P}_z \end{bmatrix} &= [\boldsymbol{S}_P \boldsymbol{M}_B + \boldsymbol{S}_L \boldsymbol{H}_B] \begin{bmatrix} \boldsymbol{v}_B \\ \boldsymbol{\omega}_B \end{bmatrix} \\ &\quad + \boldsymbol{S}_P \mathcal{P}_{feet} + \boldsymbol{S}_L \mathcal{L}_{feet} \end{aligned} \tag{20}$$

The reference momentum corresponding to the desired CoM trajectory is obtained by

$$\begin{bmatrix} \mathcal{L}_{x0}^d \\ \mathcal{L}_{y0}^d \\ \mathcal{P}_z^d \end{bmatrix} = \boldsymbol{S}_P \mathcal{P}^d. \tag{21}$$

Therefore the velocity of the pelvis link is given by

$$\begin{bmatrix} \boldsymbol{v}_B \\ \boldsymbol{\omega}_B \end{bmatrix} = [\boldsymbol{S}_P \boldsymbol{M}_B + \boldsymbol{S}_L \boldsymbol{H}_B]^\dagger \cdot \left(\boldsymbol{S}_P(\mathcal{P}^d - \mathcal{P}_{feet}) + \boldsymbol{S}_L \mathcal{L}_{feet}\right). \quad (22)$$

VI. Joint Speed of Running Pattern

Figure 13 shows the leg joint speed of the running pattern of 3 [km/h] created by the proposed algorithm. It indicates joint velocity of knees, ankle pitch joints and toe joints from top to the bottom. Since the knee and the ankle joints are driven by servo motors, they have speed limits determined by the power supply voltage. Those limitations are indicated by the horizontal dashed lines. Since the joint speeds are within limits, the planned running pattern can be realized by the actual hardware.

Before lift-off, the toe joint speed exceeds 700 [deg/s] which is two times faster than knees and ankles. Moreover, immediately after the lift-off, it becomes zero. This is possible since the toe joints are driven by springs and are equipped with mechanical hard stop.

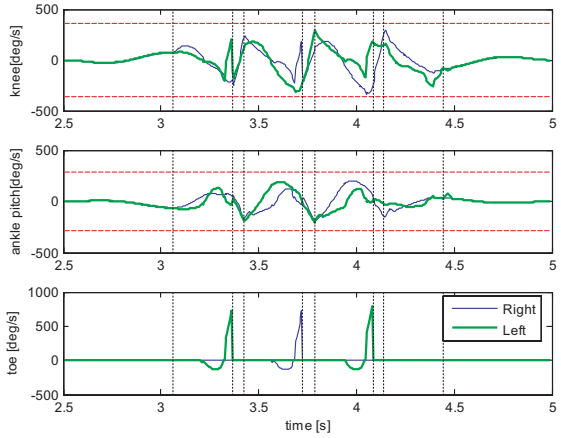

Fig. 13. Joint speed at running with toe

For comparison, we made a running pattern which does not use toes, but have identical CoM trajectory. Figure 14 shows the resulted joint speed. In this case, the knees and the ankles break the speed limits (horizontal dashed lines), therefore this running pattern cannot be realized.

VII. Simulation and Experiment

Figure 15 shows the snapshots of an open-loop dynamic simulation using the running pattern of 3 [km/h]. In the simulation, we applied PD control to all joints except toes, and the prescribed running pattern was given as their reference. The passive toe behavior was calculated in the dynamic simulation. As in the figure, we obtained the expected running with passive toes.

As the preliminary experiment, we designed a hopping by both feet for one time [3]. Since both toe springs are used

[3]A jump with both feet was also tested in our previous work using a robot without toe [12]. However, the realized flight height was only a few millimeters.

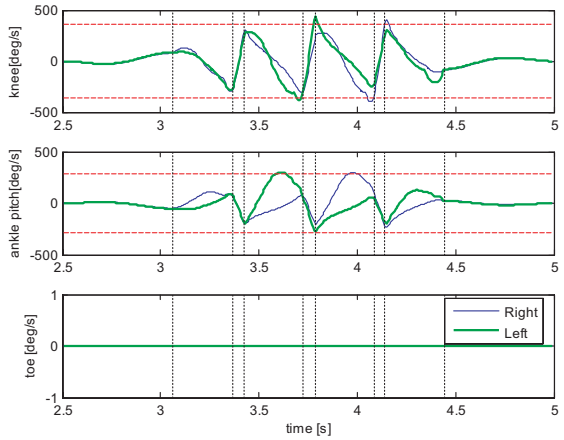

Fig. 14. Joint speed at running without using toe

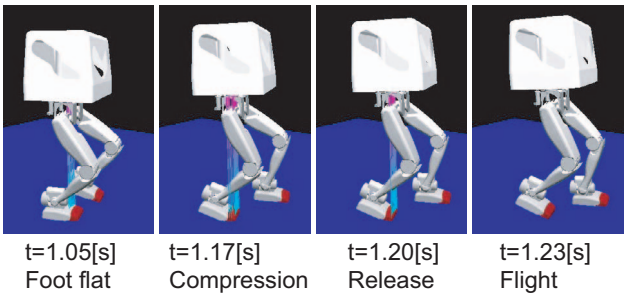

Fig. 15. Simulated running with toe springs

in parallel, we used the spring constant of $2k_{toe}$ for the algorithm of section IV. The planned joint trajectory was given as the servo reference for the HRP-2LT. Except local joint feedback, no sensor feedback was applied. Figure 16 shows the video captured frames of the experiment. We can observe the compression phase (b), the release phase (c), and the flight phase (d).

The vertical floor reaction force sensed by the foot force sensors are shown in Fig. 17. From this graph we can see the apparent flight phase of about 0.1[s] as planned. The fluctuation during flight time caused by the mass of feet under the force sensors.

VIII. Conclusion

We discussed a ZMP-based running pattern generation for a biped robot with toe springs. The trajectory of the center of mass was designed to realize the specified running motion and the foot trajectories are determined to get proper spring action at lift off phases. They were interpreted into joint angles by using a modified resolved momentum control. By using the proposed method we could realize a running at 3[km/h] in simulation. We also conducted a preliminary experiment of one time hopping motion with both legs. Our robot HRP-2LR could successfully jump by using toe springs.

As our next target, we will design and implement a controller to stabilize the running of 3[km/h] in the near future.

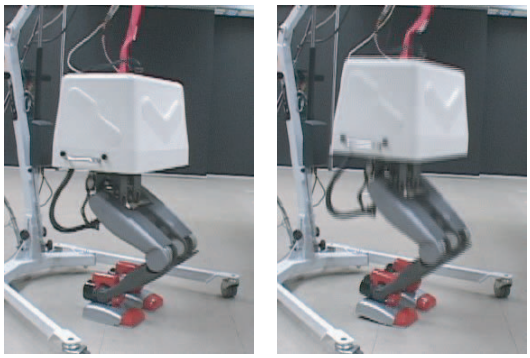

Fig. 16. Jump enhanced by toe joint

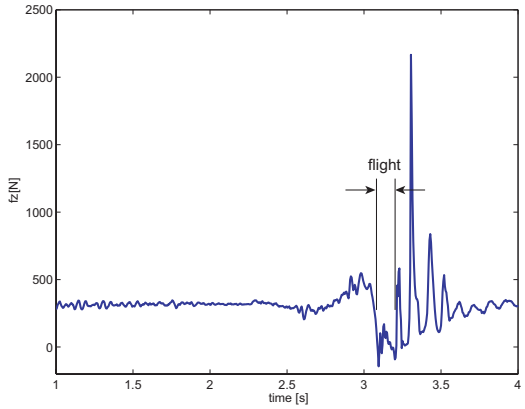

Fig. 17. Vertical reaction force

ACKNOWLEDGMENTS

We thank people of Kawada Industries, Inc. especially Jiro Sakurai, Toshikazu Kawasaki and Takakatsu Isozumi for their technical support. We also thank Fumio Kanehiro, Kiyoshi Fujiwara, Kensuke Harada and Hajime Saito of Humanoid Research Group, AIST for their kind help and excellent advice.

REFERENCES

[1] M. Gienger, F. Löffler, and F. Pfeiffer. Toward the design of a biped jogging robot. *Proc. of the 2001 ICRA*, pages 4140–4145, 2001.

[2] K. Hirai, M. Hirose, Y. Haikawa, and T. Takenaka. The development of honda humanoid robot. *Proc. of the 1998 ICRA*, pages 1321–1326, 1998.

[3] H. Inoue, S. Tachi, Y. Nakamura, K. Hirai, et al. Overview of humanoid robotics project of meti. *Proc. Int. Symp. Robotics*, pages 1478–1482, 2001.

[4] K. Nishiwaki, T. Sugihara, S. Kagami, F. Kanehiro, M. Inaba, and H. Inoue. Design and development of research platform for perception-action integration in humanoid robot: H6. *Proc. Int. Conference on Intelligent Robots and Systems*, pages 1559–1564, 2000.

[5] J. Yamaguchi, E. Soga, S. Inoue, and A. Takanishi. Development of a bipedal humanoid robot – control method of whole body cooperative dynamic biped walking –. *Proc. of the 1999 ICRA*, pages 368–374, 1999.

[6] J. Kim and J. Oh. Walking control of the humanoid platform khr-1 based on torque feedback control. *Proc. of the 2004 ICRA*, pages 623–628, 2004.

[7] M. Raibert. *Legged Robots that Balance*. MIT Press, Cambridge, MA, 1986.

[8] Robert R. Playter and Marc H. Raibert. Control of a biped somersault in 3d. *Proc. of IFToMM-jc International Symposium on Theory of Machines and Mechanisms (in Nagoya, Japan)*, pages 669–674, 1992.

[9] J. K. Hodgins. Three-dimensional human running. *Proc. of the 1996 ICRA*, pages 3271–3277, 1996.

[10] M. Ahmadi and M. Buehler. The arl monopod ii running robot: Control and energetics. *Proc. of the 1999 ICRA*, pages 1689–1694, 1999.

[11] K. Nagasaka, Y. Kuroki, S. Suzuki, Y. Itoh, and J. Yamaguchi. Integrated motion control for walking, jumping and running on a small bipedal entertainment robot. *Proc. of the 2004 ICRA*, pages 3189–3194, 2004.

[12] S. Kajita, T.Nagasaki, et al. A hop towards running humanoid biped. *ICRA*, pages 629–635, 2004.

[13] C. Chevallereau, E.R. Westervelt, and J.W. Grizzle. Asymptotically stable running for a five-link, four-actuator, planar bipedal robot. *Intr. J. of Robotics Research*, 24(6):431–464, 2005.

[14] Miomir Vukobratović and J.Stepanenko. On the stability of anthropomorphic systems. *Mathematical Biosciences*, 15:1–37, 1972.

[15] T. Nagasaki, S. Kajita, K. Kaneko, et al. A running experiment of humanoid biped. *Proc. of IROS2004*, pages 136–141, 2004.

[16] S. Kagami, K. Nishiwaki, T. Kitagawa, T. Sugihara, M. Inaba, and H. Inoue. A fast generation method of a dynamically stable humanoid robot trajectory with enhanced zmp constraint. *Proc. of Int. Conference on Huanoid Robotics*, 2000.

[17] Ramzi Sellaouti, Olivier Stasse, et al. Faster and smoother walking of humanoid hrp-2 with compliant toe joints. *Proc. of IROS2006 (to appear)*, 2006.

[18] S. Kajita, F. Kanehiro, K. Kaneko, K. Fujiwara, K. Harada, K. Yokoi, and H. Hirukawa. Resolved momentum control: Humanoid motion planning based on the linear and angular momentum. *Proc. of the 2003 IROS*, pages 1644–1650, 2003.